Hydrogenic Defects in Ferromagnetic $Cu_3(HITP)_2$ (HITP $\equiv 2,3,6,7,10,11$ -Hexaiminotriphenylene), a 2D Metal—Organic Framework

Tekalign T. Debela* and Christopher H. Hendon*



Downloaded via UNIV OF OREGON on June 3, 2024 at 19:01:11 (UTC). See https://pubs.acs.org/sharingguidelines for options on how to legitimately share published articles.

Cite This: ACS Materials Lett. 2024, 6, 2698-2702

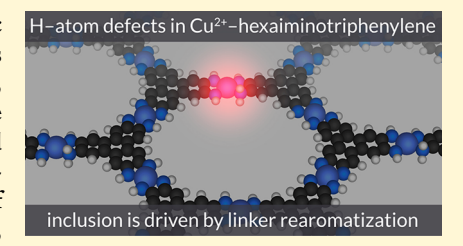


ACCESS

Metrics & More

Article Recommendations

ABSTRACT: Like all conductive materials, electrically conductive metal—organic frameworks glean their properties from their defects. Owing to the synthesis conditions required to form the peak-performing triphenylene-based conductors, adatomic H atoms are likely the most prevalent defect and may occur in the charge state of -1, 0, and +1. However, some forms of these defects necessitate unpaired electrons, and the interplay between the ligand-centered unpaired electron and spin-polarized metals remains unknown. Here, we report the formation energies of hydrogenic defects in $\text{Cu}_3(\text{HITP})_2$ (HITP $\equiv 2,3,6,7,10,11$ -hexaiminotriphenylene), the Cu^{2+} analogue of $\text{Ni}_3(\text{HITP})_2$, and show that they are comparable to the Ni^{2+}



system. d⁹ Cu²⁺ does not appreciably affect the electronic band properties of the defective framework.

onductive metal—organic frameworks $(MOFs)^{1-3}$ differentiate themselves from their typically insulating counterparts due to their delocalization of holes and electrons. The champion conductors are 2D-connected and typically consist of tri- and tetratopic π -conjugated organic ligands bound to early transition metal ions (e.g., Ni^{2+} , Cu^{2+} , Co^{2+}), forming van der Waals (vdW)-stacked crystals with conduction occurring in either the π -stacked or covalent directions, depending on composition. These frameworks show promise for applications in energy storage technologies, as sensors, $^{10-12}$ and in electrocatalysis $^{13-15}$ but are plagued by sample-to-sample variability in conductivity and show thermally activated transport when theory predicts metallicity. 16

This activated transport has been attributed to defects, including barriers associated with intergranular hopping in polycrystalline samples, ¹⁷ stacking faults, ^{18,19} poor crystallinity, ^{20–25} or chemical defects and doping. ²⁶ Additionally, other papers have suggested that the binding of a monotopic ligand to axial open metal sites may also lead to the emergence of a gap. ^{27,28} All of these factors pose problems for realizing structure—function relationships because lower than expected electrical conduction could be a product of a combination of defects.

In a recent paper,²⁶ interstitial H atoms were offered as a chemical origin for the emergence of a narrow band gap in otherwise theory-predicted metallic Ni-based MOFs, Ni₃(HITP)₂ (HITP $\equiv 2,3,6,7,10,11$ -hexaiminotriphenylene)²⁹

and Ni $_3$ (HIB) $_2$ (HIB \equiv hexaiminobenzene). While the H atom inclusion was predicted to be thermodynamically favored (negative formation energies in some conditions), the result rather suggested that during the self-assembly of the framework the linker was likely never deprotonated nor oxidized by 6H $^+$ and 3e $^-$ per ligand as illustrated in Scheme 1. This oxidation and charge state was rather inferred to achieve charge neutrality and maximize symmetry, but an identical charge is also obtained by removing only 5H $^+$ and 2e $^-$. Theory predicted that the effect was observed equally in models that contained only monolayers as well as bulk π -stacks, indicating that the monolayer models were sufficient to predict bulk defect formation energies and resultant properties.

The effect of adding a single H^{\bullet} per linker results in aromatization of one arm of the HITP linker, and desymmetrizes the π -system. While aromaticity itself is predicted to be inversely related to material conductivity, ³¹ it is also the reason that the removal of the third electron is thermodynamically disfavored. However, these materials are thought to have largely covalent

Received: April 30, 2024 Revised: May 24, 2024 Accepted: May 28, 2024



Scheme 1. (a) Schematic Representation of Hexagonal $Cu_3(HITP)_2$; (b) The Neutral Framework is Assumed to Have Linkers with Local D_{3h} Symmetry; (c) Addition of an Adatomic H $^{\bullet}$ Results in the Same Charge, but Rearomatizing One Ring and Reducing Linker Symmetry to C_s

metal—ligand bonding, suggesting that the metal—ligand electron exchange could play a role in stabilizing the $-6H^+/-3e^-$ linker, motivating us to study the H atom interstitial formation energies in the $\text{Cu}_3(\text{HITP})_2$ analogue.³² The Cu material has been reported to be less conductive than $\text{Ni}_3(\text{HITP})_2$,³³ enabling applications in chemiresistive sensing, and further, because each Cu center hosts a single unpaired electron, there is also the possibility of exotic magnetic coupling affecting defect formation.

In this study, we investigate the energy of forming hydrogenic defects in Cu₃(HITP)₂, as shown in Figure 1a. Both Ni²⁺ and Cu²⁺ can distort to form non-square-planar coordination

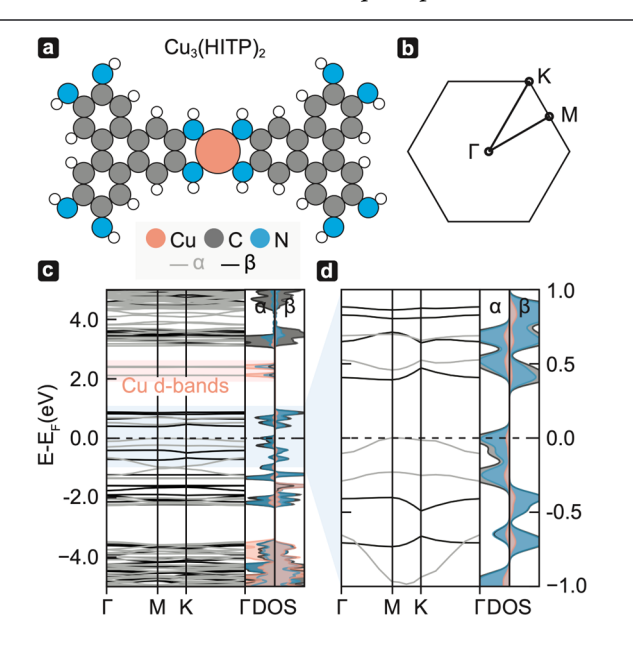


Figure 1. (a) Geometric configuration of 2D $Cu_3(HITP)_2$, (b) Brillouin zone of the hexagonal lattice, and (c, d) electronic band structure of the pristine monolayer $Cu_3(HITP)_2$ plotted at different energy ranges. Cu unoccupied d-bands are emphasized in tangerine. Γ , M, and K correspond to K-vectors of [0,0,0], [1/2,0,0], and [1/3,1/3,0], respectively.

environments. The frameworks, however, necessitate near-planar ligation, and the resultant structure contains near-square-planar Cu^{2+} with slightly buckled 2D sheets as observed in computational³⁴ and experimental³⁵ studies of other Cu-containing 2D MOFs. In this geometry, Cu^{2+} is S=1/2 (3d⁹) with the unpaired electron residing nominally in the $\mathrm{d}_{x^2-y^2}$ orbital. Since the unpaired electron may order magnetically, the material may be attractive in other applications such as quantum information storage, but the same electron may also partake in exchange stabilization of spin polarized defects. Additionally, it may also stabilize the $-6\mathrm{H}^+/-3\mathrm{e}^-$ ligand oxidation state, causing the Cu material to be dissimilar to the Ni framework. If so, this should be reflected in the defect formation energies for the inclusion or deletion of H atoms in the lattice.

To study the defect formation energy and resultant properties of defective monolayer Cu₃(HITP)₂, we used Density Functional Theory (DFT) as implemented in the Vienna *ab initio* Simulation Package (VASP).^{36,37} The projected augmented plane wave (PAW)³⁸ approach and the HSEsol^{39,40} functional were used with a plane-wave kinetic energy cutoff of 500 eV and a Γ -centered k-grid with $2 \times 2 \times 1$ k-point mesh. A large vacuum space of 20 Å was used in the z-direction (perpendicular to the layer) to ensure that no interaction occurs between adjacent supercells and confirmed by examination of the electrostatic potential in the vacuum region. Geometry optimization was performed until the average force per atom was <0.01 eV/Å, and the final energy change was $<10^{-6}$ eV per atom. The electronic structure calculations were all performed using the screened hybrid density functional HSE06 in combination with PBEsol (i.e., HSEsol⁴¹). The band structure calculations use the same electronic convergence criteria as those used for the geometric optimization.

To compute the equilibrium defect formation energy, $E^{t}[X^{q}]$ of a point defect X with a charge q we use

$$E^{f}[X^{q}] = E_{\text{tot}}[X^{q}] - E_{\text{tot}}[\text{bulk}] \pm \sum_{i} n_{i} \mu_{i} + q E_{\text{F}} + E_{\text{corr}}$$

where $E_{\rm tot}[X^q]$ and $E_{\rm tot}[{\rm bulk}]$ are the total energies of the defective and the host monolayer ${\rm Cu_3(HITP)_2}$, respectively, n_i is the number of defects (\pm for adding and removing atoms depending on the nature of the defect), and μ_i is the corresponding chemical potential of competing phases for that defect. Here we use the same chemical potentials as presented in ref 26. $E_{\rm F}$ is the Fermi energy, and $E_{\rm corr}$ is the correction term accounting for spurious image-charge Coulomb interaction between the charged defect and its periodic image due to the electrostatic finite-size effect. We account for this correction using the Freysoldt, Neugebauer, and Van de Walle (FNV) scheme, but others approaches yield the same result. 42,43

Like Ni₃(HITP)₂, the structure of monolayer Cu₃(HITP)₂ is a honeycomb lattice; the key portion presented in Figure 1a contains two linkers each having presumably lost 6H^+ and 3e^- during self-assembly. Cu₃(HITP)₂ is predicted to be a narrow band gap semiconductor with a band gap of 0.39 eV, slightly larger than that of monolayer Ni₃(HITP)₂ (~0.21 eV).²⁶ This is revealed in our electronic band structure when sampling the *k*-points of the irreducible Brillouin zone, Figure 1b,c. Further analysis of the band gap, Figure 1d, shows that the highly localized bands centered on Cu atoms sit deep within the valence band (-4 eV) from $E_{\rm F}$, suggesting that the additional Cu d-electron is not oxidizing/delocalizing into the ligand to partially aromatize the ring. Conversely, the addition of extra electrons (either coupled with protons or introduced in other

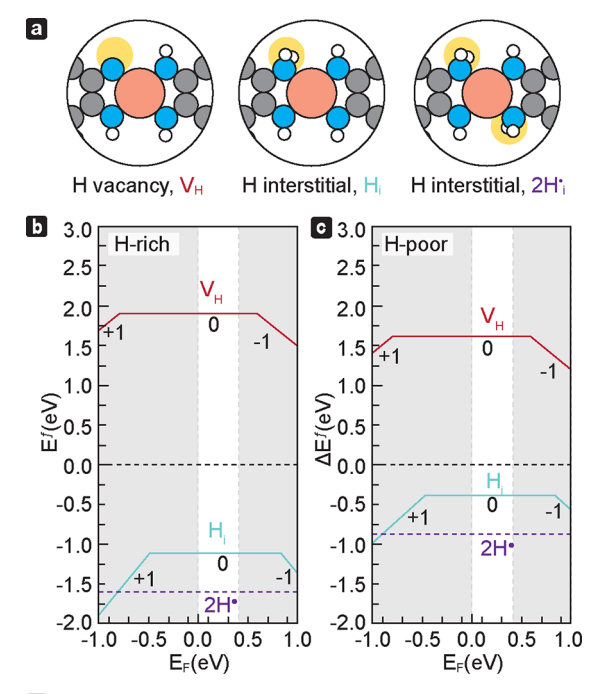
ways) are likely to not populate the unoccupied Cu d-state without other major structural perturbation, as it sit \sim 2 eV above the Fermi level. In other words, the Cu centers are acting as isolated Lewis acids, and H atom defects alone are likely not responsible for Cu⁺ defects without other correlated defects. Together, we expect that the defect formation energies should then closely mimic Ni₃(HITP)₂, but they may still interact with these unpaired electrons in some way.

We note that the electronic band structure of $Cu_3(HITP)_2$ in the literature has been reported to be metallic. ³⁴ In that study, a spin-restricted calculation was conducted at the PBE level of theory. This result is likely aphysical, as it forces the system to half populate a band because the unit cell necessitates an unpaired electron. It requires a spin-polarized calculation and a higher level of theory to accurately capture electronic properties of the $Cu_3(HITP)_2$ monolayer. We reproduced the PBE result, and circumvented the issue by (i) using the HSEsol functional for all calculations and (ii) sampling the magnetic ordering using a 2 \times 2 supercell. The latter revealed that a ferromagnetic delectron configuration was 0.01 eV more stable than that of the antiferromagnetic analogue. The same calculation also allowed us to continue our simulations using the three Cu atom containing unit cell and enforcing the ferromagnetic order.

Since the 2D Cu₃(HITP)₂ monolayer is a narrow gap semiconductor, the formation energy of defects depends on both $E_{\rm F}$ and the charge of the defect and its location within the crystal. During the nucleation of the crystal shown in Scheme 1, the framework assembles, with deprotonation and oxidation of the linker occurring throughout. While unlikely, there is a chance that the linker was over-deprotonated in the process, a vacancy of H. Here, the formation energy of the product of that reaction, a hydrogen vacancy (V_H) in reasonable charge states, q= -1, 0 (\bullet), and +1, is shown in Figure 2b,c. Aligning with our intuition, a seventh deprotonation is highly unlikely (i.e., V_H , q =-1; defect formation energies ranging from \sim 2.5 to 3.0 eV and deep in the conduction band, depending on the H potential). Similarly, the hydrogen vacancy at the q = +1 charge state is also not favorable as it is deep inside the valence band. The deletion of a single H atom is marginally more favorable ($E^{f} = 1.6-2 \text{ eV}$ depending on the chemical potential of H used). At this formation energy, this defect is expected to be extremely dilute, essentially nonexistent.

Instead, a more likely defect is one that either acts on the inherent basicity of the amines (i.e., interstitial H⁺) or reduces the framework and rearomatizes the HITP ring(s) (i.e., interstitial H[•] and H⁻). The formation energies of the hydrogen interstitials (H_i) in monolayer Cu₃(HITP)₂ under both hydrogen-rich and hydrogen-poor conditions are also presented in Figure 2b,c. From these energies, their formation energies for all charge states are very low, indicating a high thermodynamic stability for H_i in this MOF. In particular, the 2H[•] interstitial configuration (depicted in Figure 2a) yields the most negative formation energies. In addition, the electronic structure of Cu₃(HITP)₂ with 2H[•] interstitials exhibits semiconductor behavior with a band gap of 0.71 eV as shown in Figure 2d. The near doubling of the electronic gap is an effect that should be experimentally observable either spectroscopically or through examination of the activation barriers for charge conduction.

With interstitial H of varying charge, electrons are redistributed about the N-donor atoms. There is also a corresponding metal—ligand bond expansion with an increase in electron density on the donor atoms. From the Bader analysis presented in Figure 3a, the charge density on the N-donor atoms



d Electronic band structure of 2H interstitials

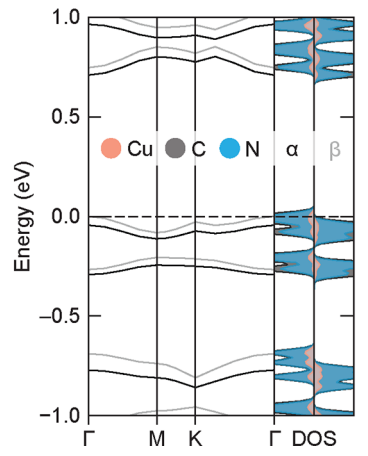


Figure 2. (a) Atomic configuration showing the hydrogen vacancy (V_H) , interstitial hydrogen (H_i) , and $2H_i$. Defect formation energies for hydrogenic defects in $Cu_3(HITP)_2$: (b) hydrogen vacancy and (c) interstitials in different charge states reveal that interstitial hydrogen is predicted to spontaneously form as H^+ and H^{\bullet} . The addition of $2H^{\bullet}$ (one per linker) is the most favorable, as it rearomatizes both ligands. (d) Resultant electronic band structure showing a 0.71 eV electronic band gap.

shifts depending on whether 0, 1, or 2 additional electrons are added to the computational cell. Notably, with the addition of H^+ , the charge on the host N atom decreases. The addition of a H^{\bullet} results in rearomatization of one ring, reflected in an equalization of the charge on both N centers. The addition of a second electron (i.e., H^-) results in a symmetrization of the charge across the metal interface, independent of the position of the H nuclei. This further supports our hypothesis that ring aromatization is a strong driving force during self-assembly. In all cases, ferromagnetically ordered spins remain favored by 0.01 eV.

The corresponding electronic band structures for each adatomic defect are also presented in Figure 3. From these data, it is clear that a single H[•] atom results in a semiconductor with a direct band gap of 0.27 eV at the M point. The cell has an

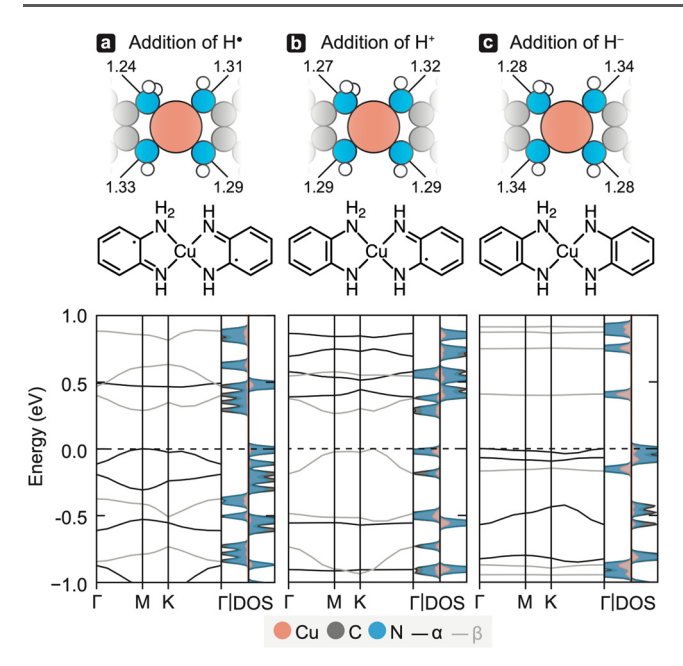


Figure 3. Electronic band structures of symmetry reduced single atom additions of H interstitials in $\operatorname{Cu}_3(\operatorname{HITP})_2$ in charge states q=0 (\bullet), +1, and -1, in panels a, b, and c, respectively. Bader charges are presented for each N atom, and their corresponding bonding schematic is shown to rationalize the redistribution of electrons. With no adatomic H, the Bader charge is computed to be 1.29 for all N sites.

even number of electrons and ferromagnetic ordering. On the other hand, the addition of a H^+ only breaks the symmetry while maintaining unpaired electrons, interestingly rendering the framework semiconducting rather than metallic, as demonstrated by the direct narrow band gap (0.26 eV) shown in Figure 3b. Incorporating H^- slightly increases the band gap to 0.4 eV.

Together, these data suggest that $Cu_3(HITP)_2$ is tolerant to H atom defects in the sense that their inclusion in the monolayer is not expected to grossly affect the material's properties. The study also illustrates that the defects in these materials are driven by linker chemistry, and there is essentially no dependence on metal identity in governing the installation of H atom defects in the framework. The defect formation energies of the hydrogenic defects are similar to those found in Ni₃(HITP)₂, suggesting that the Cu d-electrons are not interacting with the unpaired electrons on the linkers. Finally, thinking broadly about wellcharacterized defects in these materials, the most prevalent is the emergence of Cu⁺. This poses an interesting question of how Cu²⁺ reduction is likely not correlated with H atom inclusion, given that the electronic band structure reveals that the Cu dstates sit well above other ligand centered bands. We are left pondering whether the Cu⁺ defect is correlated to linker vacancies or other compositional and structural defects.

AUTHOR INFORMATION

Corresponding Authors

Tekalign T. Debela — Department of Chemistry and Biochemistry, University of Oregon, Eugene, Oregon 97403, United States; Email: debelatt@uoregon.edu

Christopher H. Hendon — Department of Chemistry and Biochemistry, University of Oregon, Eugene, Oregon 97403, United States; orcid.org/0000-0002-7132-768X; Email: chendon@uoregon.edu

Complete contact information is available at: https://pubs.acs.org/10.1021/acsmaterialslett.4c00923

Author Contributions

The manuscript was written by T.T.D. and C.H.H. DFT calculations were performed by all authors.

Notes

The authors declare no competing financial interest.

ACKNOWLEDGMENTS

This material is based upon work supported by the National Science Foundation through the Division of Materials Research under Grant DMR-1956403 and support from the Camille and Henry Dreyfus Foundation. This work used Expanse at SDSC through allocation CHE160003 from the Advanced Cyberinfrastructure Coordination Ecosystem: Services and Support (ACCESS) program, which is supported by the National Science Foundation grants #2138259, #2138286, #2138307, #2137603, and #2138296.

■ REFERENCES

- (1) Ko, M.; Mendecki, L.; Mirica, K. A. Conductive Two-Dimensional Metal—Organic Frameworks as Multifunctional Materials. *Chem. Commun.* **2018**, *54*, 7873—7891.
- (2) Xie, L. S.; Skorupskii, G.; Dincă, M. Electrically Conductive Metal-Organic Frameworks. *Chem. Rev.* **2020**, *120*, 8536–8580.
- (3) Zhang, X.; Zhou, Y.; Cui, B.; Zhao, M.; Liu, F. Theoretical Discovery of a Superconducting Two-Dimensional Metal—Organic Framework. *Nano Lett.* **2017**, *17*, 6166–6170.
- (4) Wang, M.; Dong, R.; Feng, X. Two-Dimensional Conjugated Metal—Organic Frameworks (2D c-MOFs): Chemistry and Function for MOFtronics. *Chem. Soc. Rev.* **2021**, *50*, 2764—2793.
- (5) Meng, Z.; Jones, C. G.; Farid, S.; Khan, I. U.; Nelson, H. M.; Mirica, K. A. Unraveling the Electrical and Magnetic Properties of Layered Conductive Metal-Organic Framework With Atomic Precision. *Angew. Chem., Int. Ed.* **2022**, *61*, No. e202113569.
- (6) Feng, D.; Lei, T.; Lukatskaya, M. R.; Park, J.; Huang, Z.; Lee, M.; Shaw, L.; Chen, S.; Yakovenko, A. A.; Kulkarni, A.; Xiao, J.; Fredrickson, K.; Tok, J. B.; Zou, X.; Cui, Y.; Bao, Z. Robust and Conductive Two-Dimensional Metal—organic Frameworks with Exceptionally High Volumetric and Areal Capacitance. *Nat. Energy* **2018**, *3*, 30–36.
- (7) Wu, Z.; Adekoya, D.; Huang, X.; Kiefel, M. J.; Xie, J.; Xu, W.; Zhang, Q.; Zhu, D.; Zhang, S. Highly Conductive Two-Dimensional Metal—Organic Frameworks for Resilient Lithium Storage with Superb Rate Capability. *ACS Nano* **2020**, *14*, 12016—12026.
- (8) Suman, S. P.; Dontireddy, G. M. R.; Chen, T.; Wang, J.; Dou, J.-H.; Banda, H. Enhanced Redox Storage and Diverse Intercalation in Layered Metal Organic Frameworks with a Staggered Stacking Mode. *ACS Energy Lett.* **2024**, *9*, 1572–1580.
- (9) Yuan, D.; Dou, Y.; Wu, Z.; Tian, Y.; Ye, K.-H.; Lin, Z.; Dou, S. X.; Zhang, S. Atomically Thin Materials for Next-Generation Rechargeable Batteries. *Chem. Rev.* **2022**, *122*, 957–999.
- (10) Park, C.; Baek, J. W.; Shin, E.; Kim, I.-D. Two-Dimensional Electrically Conductive Metal—Organic Frameworks as Chemiresistive Sensors. *ACS Nanosci. Au* **2023**, *3*, 353–374.
- (11) Stolz, R. M.; Mahdavi-Shakib, A.; Frederick, B. G.; Mirica, K. A. Host–Guest Interactions and Redox Activity in Layered Conductive Metal–Organic Frameworks. *Chem. Mater.* **2020**, *32*, 7639–7652.
- (12) Yao, M.; Lv, X.; Fu, Z.; Li, W.; Deng, W.; Wu, G.; Xu, G. Layer-by-Layer Assembled Conductive Metal—Organic Framework Nano-films for Room-Temperature Chemiresistive Sensing. *Angew. Chem., Int. Ed.* **2017**, *56*, 16510—16514.
- (13) Duan, J.; Chen, S.; Zhao, C. Ultrathin Metal-Organic Framework Array for Efficient Electrocatalytic Water Splitting. *Nat. Commun.* **2017**, *8*, 15341.

- (14) Clough, A. J.; Yoo, J. W.; Mecklenburg, M. H.; Marinescu, S. C. Two-Dimensional Metal—Organic Surfaces for Efficient Hydrogen Evolution from Water. *J. Am. Chem. Soc.* **2015**, *137*, 118–121.
- (15) Ji, Y.; Dong, H.; Liu, C.; Li, Y. Two-Dimensional π -Conjugated Metal—Organic Nanosheets as Single-Atom Catalysts for the Hydrogen Evolution Reaction. *Nanoscale* **2019**, *11*, 454–458.
- (16) Clough, A. J.; Skelton, J. M.; Downes, C. A.; de la Rosa, A. A.; Yoo, J. W.; Walsh, A.; Melot, B. C.; Marinescu, S. C. Metallic Conductivity in a Two-Dimensional Cobalt Dithiolene Metal—Organic Framework. *J. Am. Chem. Soc.* **2017**, *139*, 10863—10867.
- (17) Dou, J.-H.; Sun, L.; Ge, Y.; Li, W.; Hendon, C. H.; Li, J.; Gul, S.; Yano, J.; Stach, E. A.; Dincă, M. Signature of Metallic Behavior in the Metal—Organic Frameworks M $_3$ (Hexaiminobenzene) $_2$ (M = Ni, Cu). *J. Am. Chem. Soc.* **2017**, *139*, 13608–13611.
- (18) Zojer, E.; Winkler, C. Maximizing the Carrier Mobilities of Metal-Organic Frameworks Comprising Stacked Pentacene Units. *J. Phys. Chem. Lett.* **2021**, *12*, 7002–7009.
- (19) Foster, M. E.; Sohlberg, K.; Allendorf, M. D.; Talin, A. A. Unraveling the Semiconducting/Metallic Discrepancy in Ni ₃ (HITP) ₂. *J. Phys. Chem. Lett.* **2018**, *9*, 481–486.
- (20) Snook, K. M.; Zasada, L. B.; Chehada, D.; Xiao, D. J. Oxidative Control over the Morphology of Cu₃(HHTP)₂, a 2D Conductive Metal–Organic Framework. *Chem. Sci.* **2022**, *13*, 10472–10478.
- (21) Skorupskii, G.; Chanteux, G.; Le, K. N.; Stassen, I.; Hendon, C. H.; Dincă, M. Electrical Conductivity through π – π Stacking in a Two-dimensional Porous Gallium Catecholate Metal—Organic Framework. *Ann. N.Y. Acad. Sci.* **2022**, *1518*, 226–230.
- (22) Skorupskii, G.; Le, K. N.; Cordova, D. L. M.; Yang, L.; Chen, T.; Hendon, C. H.; Arguilla, M. Q.; Dincă, M. Porous Lanthanide Metal—Organic Frameworks with Metallic Conductivity. *Proc. Natl. Acad. Sci. U. S. A.* **2022**, *119*, No. e2205127119.
- (23) Skorupskii, G.; Trump, B. A.; Kasel, T. W.; Brown, C. M.; Hendon, C. H.; Dincă, M. Efficient and Tunable One-Dimensional Charge Transport in Layered Lanthanide Metal—Organic Frameworks. *Nat. Chem.* **2020**, *12*, 131—136.
- (24) Dou, J.-H.; Arguilla, M. Q.; Luo, Y.; Li, J.; Zhang, W.; Sun, L.; Mancuso, J. L.; Yang, L.; Chen, T.; Parent, L. R.; Skorupskii, G.; Libretto, N. J.; Sun, C.; Yang, M. C.; Dip, P. V.; Brignole, E. J.; Miller, J. T.; Kong, J.; Hendon, C. H.; Sun, J.; Dincă, M. Atomically Precise Single-Crystal Structures of Electrically Conducting 2D Metal—Organic Frameworks. *Nat. Mater.* 2021, 20, 222—228.
- (25) Hmadeh, M.; Lu, Z.; Liu, Z.; Gándara, F.; Furukawa, H.; Wan, S.; Augustyn, V.; Chang, R.; Liao, L.; Zhou, F.; Perre, E.; Ozolins, V.; Suenaga, K.; Duan, X.; Dunn, B.; Yamamto, Y.; Terasaki, O.; Yaghi, O. M. New Porous Crystals of Extended Metal-Catecholates. *Chem. Mater.* **2012**, *24*, 3511–3513.
- (26) Debela, T. T.; Yang, M. C.; Hendon, C. H. Ligand-Mediated Hydrogenic Defects in Two-Dimensional Electrically Conductive Metal—Organic Frameworks. *J. Am. Chem. Soc.* **2023**, *145*, 11387—11391.
- (27) Foster, M. E.; Sohlberg, K.; Spataru, C. D.; Allendorf, M. D. Proposed Modification of the Graphene Analogue $Ni_3(HITP)_2$ To Yield a Semiconducting Material. *J. Phys. Chem. C* **2016**, *120*, 15001–15008.
- (28) Le, K. N.; Mancuso, J. L.; Hendon, C. H. Electronic Challenges of Retrofitting 2D Electrically Conductive MOFs to Form 3D Conductive Lattices. ACS Appl. Electron. Mater. 2021, 3, 2017–2023.
- (29) Sheberla, D.; Sun, L.; Blood-Forsythe, M. A.; Er, S.; Wade, C. R.; Brozek, C. K.; Aspuru-Guzik, A.; Dincă, M. High Electrical Conductivity in Ni₃(2,3,6,7,10,11-Hexaiminotriphenylene)₂, a Semiconducting Metal–Organic Graphene Analogue. *J. Am. Chem. Soc.* **2014**, *136*, 8859–8862.
- (30) Dou, J.-H.; Sun, L.; Ge, Y.; Li, W.; Hendon, C. H.; Li, J.; Gul, S.; Yano, J.; Stach, E. A.; Dincă, M. Signature of Metallic Behavior in the Metal–Organic Frameworks M_3 (Hexaiminobenzene)₂ (M = Ni, Cu). *J. Am. Chem. Soc.* **2017**, *139*, 13608–13611.
- (31) Demuth, M. C.; Hendon, C. H. Linker Aromaticity Reduces Band Dispersion in 2D Conductive Metal—Organic Frameworks. *ACS Mater. Lett.* **2023**, *5*, 1476—1480.

- (32) Campbell, M. G.; Sheberla, D.; Liu, S. F.; Swager, T. M.; Dincă, M. Cu₃(hexaiminotriphenylene)₂: An Electrically Conductive 2D Metal Organic Framework for Chemiresistive Sensing. *Angew. Chem., Int. Ed.* **2015**, *54*, 4349–4352.
- (33) Mariano, R. G.; Wahab, O. J.; Rabinowitz, J. A.; Oppenheim, J.; Chen, T.; Unwin, P. R.; Dincă, M. Thousand-fold increase in O₂ electroreduction rates with conductive MOFs. *ACS Cent. Sci.* **2022**, *8*, 975–982.
- (34) Chen, S.; Dai, J.; Zeng, X. C. Metal—Organic Kagome Lattices M3(2,3,6,7,10,11-Hexaiminotriphenylene)2 (M = Ni and Cu): From Semiconducting to Metallic by Metal Substitution. *Phys. Chem. Chem. Phys.* **2015**, *17*, 5954–5958.
- (35) Park, G.; Demuth, M. C.; Hendon, C. H.; Park, S. S. Acid-Dependent Charge Transport in a Solution-Processed 2D Conductive Metal-Organic Framework. *J. Am. Chem. Soc.* **2024**, *146*, 11493–11499.
- (36) Kresse, G.; Furthmüller, J. Efficiency of Ab-Initio Total Energy Calculations for Metals and Semiconductors Using a Plane-Wave Basis Set. *Comput. Mater. Sci.* **1996**, *6*, 15–50.
- (37) Kresse, G.; Furthmüller, J. Efficient Iterative Schemes for Ab Initio Total-Energy Calculations Using a Plane-Wave Basis Set. *Phys. Rev. B* **1996**, *54*, 11169–11186.
- (38) Kresse, G.; Joubert, D. From Ultrasoft Pseudopotentials to the Projector Augmented-Wave Method. *Phys. Rev. B* **1999**, *59*, 1758–1775
- (39) Perdew, J. P.; Ruzsinszky, A.; Csonka, G. I.; Vydrov, O. A.; Scuseria, G. E.; Constantin, L. A.; Zhou, X.; Burke, K. Restoring the Density-Gradient Expansion for Exchange in Solids and Surfaces. *Phys. Rev. Lett.* **2008**, *100*, No. 136406.
- (40) Perdew, J. P.; Burke, K.; Ernzerhof, M. Generalized Gradient Approximation Made Simple. *Phys. Rev. Lett.* **1996**, *77*, 3865–3868.
- (41) Krukau, A. V.; Vydrov, O. A.; Izmaylov, A. F.; Scuseria, G. E. Influence of the Exchange Screening Parameter on the Performance of Screened Hybrid Functionals. *J. Chem. Phys.* **2006**, *125*, No. 224106.
- (42) Freysoldt, C.; Neugebauer, J.; Van de Walle, C. G. Electrostatic Interactions between Charged Defects in Supercells: Electrostatic Interactions between Charged Defects in Supercells. *Phys. Status Solidi B* **2011**, 248, 1067–1076.
- (43) Freysoldt, C.; Neugebauer, J.; Van de Walle, C. G. Fully *Ab Initio* Finite-Size Corrections for Charged-Defect Supercell Calculations. *Phys. Rev. Lett.* **2009**, *102*, No. 016402.